symmetric structure which is pseudo-centrosymmetric, and that this is the reason for the difficulty in refining the non-centrosymmetric structure.

However, it appears that the weighted residual test can suggest the incorrect non-centrosymmetric structure instead of the correct centrosymmetric one. This may possibly be due to using an incomplete model, but is most likely to originate from an ill-conditioned matrix which arises from the pseudo-symmetry of the non-centrosymmetric structure.

If the matrix is ill-conditioned, it will vitiate the weighted residual test. Because of these difficulties it would appear unwise in such cases to depend on the weighted residual test alone.

This and the previous paper incorporate work submitted by one of us (A.W.) in part fulfilment of a Ph.D. thesis of the University of London. We should like to thank the Science Research Council for support and Professor J.D. Bernal for encouragement and for facilities for carrying on the work. The help of the referee in improving the presentation of the two papers is gratefully acknowledged.

References

CRUICKSHANK, D. W. J. (1965). Private communication.
DIAMAND, R. D. (1964). Private communication.
HAMILTON, W. C. (1965). *Acta Cryst.* **18**, 502.
HAMILTON, W. C. (1966). Private communication.
HOWELLS, E. R., PHILLIPS, D. C. & ROGERS, D. (1949). *Research*, **2**, 338.
HOWELLS, E. R., PHILLIPS, D. C. & ROGERS, D. (1950). *Acta Cryst.* **3**, 210.
LIPSON, H. & WOOLFSON, M. M. (1952). *Acta Cryst.* **5**, 680.
MASON, R. (1964). *Acta Cryst.* **17**, 547.
RÜDORFF, W. & HOFMANN, U. (1935). *Z. Phys. Chem.* B, **28**, 351.
WHITAKER, A. & JEFFERY, J. W. (1967). *Acta Cryst.* **23**, 977.
WILSON, A. J. C. (1949*a*). *Research*, **2**, 246.
WILSON, A. J. C. (1949*b*). *Acta Cryst.* **2**, 318.

Acta Cryst. (1967). **23**, 989

Structure and Electron Density of 2,5-Dimethyl-*p*-benzoquinone

BY F. L. HIRSHFELD AND D. RABINOVICH

Department of Chemistry, Weizmann Institute of Science, Rehovoth, Israel

(*Received* 2 *December* 1966 *and in revised form* 12 *April* 1967)

The electron distribution in the dimethylquinone molecule has been studied by least-squares refinement of a flexible model chosen to represent the charge redistribution attendant on chemical binding. This model incorporates ellipsoidal pseudo-atoms centred at the mid points of all carbon–carbon and carbon–oxygen bonds and contracted, polarized hydrogen atoms; it assigns individually adjustable occupancy factors and anisotropic 'vibration' parameters to all heavy atoms. Results indicate a build-up of excess charge, amounting to about one-tenth electron, in the C–C bond region, drawn from localized regions on the far sides of the bonded carbon atoms; a further excess charge, of similar magnitude, in the π component of the C=C bond, with its maximum density about 0·5 Å above and below the nodal plane; no appreciable excess density in or near the C=O bond; and a sharp concentration and polarization of charge in hydrogen atoms bonded to carbon. Bond lengths and angles differ from those in the parent benzoquinone principally at the points of methyl substitution. The molecule appears to vibrate essentially as a rigid body except for an appreciable torsional oscillation of the methyl groups.

Introduction

The X-ray data collected for the crystal-structure determination of 2,5-dimethyl-*p*-benzoquinone (Rabinovich & Schmidt, 1964) have been further analysed for the information they may yield on the distribution of electron density, especially in the regions of the covalent bonds. A preliminary report (Hirshfeld, Rabinovich, Schmidt & Ubell, 1963) concentrated largely on the shape of the hydrogen peaks; the present paper deals more generally with the changes in electron density in the molecule as compared with the separate atoms of which it is composed.

Experimental data and initial refinement

The unit cell contains two molecules at non-equivalent centres of symmetry in $P\bar{1}$ and has the cell dimensions, at 25°±1°C:

$$a=4{\cdot}013,\ b=9{\cdot}366,\ \ c=9{\cdot}738\ \text{Å},$$
$$\alpha=93{\cdot}50,\ \beta=101{\cdot}36,\ \gamma=98{\cdot}57°.$$

The X-ray intensities were measured on the General Electric goniostat with nickel-filtered Cu $K\alpha$ radiation in a convergent beam of 0·6° width, which was considered adequate to permit stationary-crystal-and-counter measurement of the integrated intensities

(α_1–α_2 doublet at $2\theta < 130°$; resolved α_1 line at $130° < 2\theta < 165°$). The crystal measured $0{\cdot}25 \times 0{\cdot}25 \times 0{\cdot}20$ mm. Each measurement consisted of a ten-second count of the reflexion and a ten-second background count with the crystal offset in ω by about 1·5°. After elimination of several reflexions evidently affected by extinction or by white-radiation background and of all fifth-order reflexions, subject to interference by Fe $K\alpha$ contamination of the radiation, there remained 1548 acceptable observations, including 194 reflexions that had $F^2 < \sigma(F^2)$ and were treated as unobserved with $F_t^2 = \sigma(F^2)$.

The initial study comprised the refinement, by diagonal least-squares methods, of the coordinates and thermal parameters of the 18 atoms (two half-molecules) in the asymmetric unit. The eight carbon and two oxygen atoms were treated in standard fashion, with three coordinates and six anisotropic vibration parameters per atom, all independently adjustable. In the early work (Rabinovich & Schmidt, 1964) the hydrogen atoms had been treated isotropically, but later a special computer routine was written to circumvent the dilemma of either imposing isotropic vibration on the hydrogen atoms or allowing each of them six independent anisotropic vibration parameters. The model adopted assigned to each hydrogen atom a vibration tensor compounded of three contributions: the motion imparted by the translation and libration of the molecule to which it belongs; a torsional oscillation of the methyl group about its exocyclic C–C bond (for methyl hydrogen atoms only); and internal stretching and bending vibrations of the C–H bond. The translation and libration tensors **T** and **ω** of both molecules were derived in the usual way (Cruickshank, 1956) from the vibration components U^{ij} of their carbon and oxygen atoms; these led to calculated vibration tensors for the several hydrogen atoms due to the general molecular motion. The torsional motion was assumed to impart to each methyl hydrogen an additional mean square displacement in the tangential direction (perpendicular both to the C–H bond and to the exocyclic C–C bond) whose magnitude was given, for all six methyl hydrogen atoms, by the single adjustable parameter U_t. Finally, the internal C–H vibrations were represented by a vibration ellipsoid for each hydrogen atom, axially symmetric about the C–H bond axis with mean square amplitudes U_a along the bond axis and U_n normal to this axis. The magnitudes of U_a and U_n were taken as adjustable parameters, identical for all hydrogen atoms, aliphatic as well as olefinic. The tensors representing the rigid-body motion, the torsional motion, and the C–H vibrations were summed algebraically for each hydrogen atom. This model, with only three adjustable vibration parameters (U_a, U_n, and U_t) for the eight hydrogen atoms, yielded a slightly better agreement ($r = 0{\cdot}0123$ compared with 0·0141) than the model assigning eight independent isotropic vibration parameters to these atoms.

This stage of the study used a hydrogen *f* curve based on the free-atom 1*s* wave function. Any change in the atomic charge cloud due to bond formation could express itself only *via* the C–H 'vibration' parameters U_a and U_n. Thus it was no surprise that these parameters refined to negative values $U_a = -0{\cdot}023 \pm 0{\cdot}007$ and $U_n = -0{\cdot}027 \pm 0{\cdot}006$ Å^2, indicating a contraction of the hydrogen charge cloud, compared with that of the isolated atom, that more than masked the zero-point stretching and bending vibrations.

A difference map evaluated in the mean planes of the two molecules showed well-rounded peaks at the midpoints of all carbon–carbon bonds, with peak densities about 0·2 e.Å^{-3}. Perpendicular sections through the bond axes showed the C=C double bonds to have slightly more elongated peaks than the single bonds. No peaks or other significant features were found in the C=O bonds or near the oxygen atoms. It was this difference map, together with the behavior of the hydrogen 'vibration' parameters, that prompted an attempt to characterize more systematically the changes in electron distribution brought about by the molecular binding.

Least-squares program

This work was facilitated by the development of a versatile least-squares refinement program, written in Fortran for the Control Data Corporation 1604-A computer with 32K storage. It offers a choice of full-matrix or flexible block-diagonal refinement and provides the following special options:

(1) The vibration components U^{ij} of each atom may be either refined independently in the usual way or made to depend on a set of molecular translation and libration components T^{ij} and ω_{ij}; the latter may be refined as subsidiary parameters along with the atomic coordinates, *etc.* in a combined iterative least-squares procedure (Hirshfeld & Rabinovich, 1966).

(2) Selected atoms may be assigned fixed or variable cylindrical coordinates in a local coordinate system defined with respect to specified neighboring atoms. The vibration ellipsoid of such an atom may be constrained to be diagonal in its local coordinate system or, more generally, to be compounded of a locally diagonal tensor superimposed algebraically on the vibration ellipsoid due to the translational and librational motion of the appropriate molecule. The coordinates and vibration parameters, in their respective local systems, of several similar atoms can be made equal to each other and refined together. By this means, for example, the coordinates and vibration parameters of the six methyl hydrogen atoms could be made to depend on four refinable positional parameters (the C–H bond length, the C–C–H angle, and, in each molecule, an azimuth angle about the C–C bond) and the three vibration parameters U_a, U_n, and U_t defined above. Similarly, the excess charge clouds in the bonds were represented by pseudo-atoms centred at the mid points of the several carbon–carbon and carbon–oxygen bonds with ellipsoidal charge densities

$$\varrho(\xi,\zeta,\eta)=[q/a_1a_2a_3(2\pi)^{3/2}] \exp[-(\xi^2/2a_1^2)-(\zeta^2/2a_2^2)-(\eta^2/2a_3^2)] .$$

The principal axes ξ,ζ,η of each of these ellipsoids were fixed, respectively, along the bond axis, perpendicular to the bond in the mean molecular plane, and normal to this plane. The total charge q and the Gaussian width parameters a_i^2 were formally equivalent to an occupancy factor and three orthogonal vibration parameters of a point atom of unit charge.

(3) Complex scattering factors are available for the hydrogen atoms, based on an axially symmetric charge density

$$\varrho(r,z)=[\lambda^3/\pi a_0^3(1+\mu^2)](1+\mu\lambda z/a_0)^2\exp(-2\lambda r/a_0) ,$$

where r is the distance from the nucleus and z is the component of this distance along an axis directed towards the adjacent carbon atom. The orbital exponent λ and the hybridization ratio μ are additional parameters subject to least-squares refinement. For such a charge distribution the scattering factor is

$$f(\mathbf{s})=\frac{1}{1+\mu^2}\left[\frac{1+\mu^2+x^2}{(1+x^2)^3}-\frac{\mu^2x^2\cos^2\chi}{(1+x^2)^4}+\frac{4i\mu x\cos\chi}{(1+x^2)^3}\right],$$

where $x=\pi a_0 s/\lambda$ and χ is the angle between the reciprocal vector $\mathbf{s}$ and the z axis. Derivation of this formula follows the procedure outlined by McWeeny (1951).

Alternative refinements

Several alternative models of varying flexibility were refined by full-matrix calculations in which the weighted residual

$$r=\Sigma w(k^2F_o^2-|F_c|^2)^2/\Sigma wk^4F_o^4$$

was iteratively minimized. The summations included 1354 observed reflexions plus, in each refinement cycle, those of the 194 unobserved for which $kF_t<|F_c|$, where F_t is the threshold value of the reflexion. Each refinement was carried to a high degree of convergence, with the calculated shifts reduced, in almost all cases, to well under one tenth of the corresponding e.s.d. Data on the most important of these models are summarized in Table 1.

All models except $A1$, $B1$, and $C1$ treated as independently adjustable a common set of 53 parameters, denoted by the column heading 'other'. These are the x,y,z coordinates of the eight carbon and two oxygen atoms; the aliphatic C–C–H and olefinic C=C–H angles α_A and α_O, and the methyl azimuth angles ψ in the two molecules; the hydrogen orbital exponent λ and hybridization ratio μ, identical values being assumed for aliphatic and olefinic hydrogen, and the tangential mean square displacement U_t of the methyl hydrogen atoms; and the charge q and Gaussian parameters a_1^2,a_2^2,a_3^2 of the four types of bond cloud (C=O, exocyclic C–C, endocyclic C–C, and C=C). In models D and E the two non-equivalent pairs of endocyclic C–C bond cloud were treated independently, raising the number of 'other' parameters to 57. The several models differ in their treatment of the carbon and oxygen vibration parameters U^{ij}, their occupancy factors A, the aliphatic and olefinic C–H bond lengths l_A and l_O, and the C–H stretching and bending parameters U_a and U_n. The following alternative procedures were followed:

The 10×6 vibration parameters U^{ij} of carbon and oxygen were either refined independently (indicated by '60' under column heading $U^{ij}_{C,O}$) or evaluated as explicit functions of the molecular tensors $\mathbf{T}$ and $\boldsymbol{\omega}$ ('24' in same column). In the latter case the six translation and six libration components of each of the two molecules were refined.

The carbon and oxygen occupancy factors were either refined independently ('10' under heading $A_{C,O}$) or fixed at unity. If refined, they were jointly rescaled after each cycle, together with the bond-cloud charges q and the scale factor k, to maintain the correct total electron count. If the occupancy factors were fixed, k was refined normally ('1' under $A_{C,O}$).

The C–H bond lengths l_A and l_O were either refined ('2' under l_{C-H}) or fixed near the supposed true internuclear distances.

Finally, the hydrogen mean square stretching and bending amplitudes ($U_{A,a}$ and $U_{A,n}$ for aliphatic C–H, and $U_{O,a}$, $U_{O,n1}$, and $U_{O,n2}$ for olefinic C–H, where $n1$ and $n2$ refer, respectively, to in-plane and out-of-plane bending) were either refined ('5' under $U_{a,n}$) or assigned fixed values based on reported infrared frequencies.

Table 1. *Numbers of independent parameters varied in several alternative refinements and corresponding discrepancy indices*

See text for explanation of various parameters.

Model	$U^{ij}_{C,O}$	$A_{C,O}$	l_{C-H}	$U_{a,n}$	Other	Total	10^5r	10^4R
A	60	1	—	—	53	114	755	419
*A*1	24	(fixed values from model *A*)				(24)	880	443
*A*2	24	1	—	—	53	78	862	439
B	60	10	—	—	53	123	707	399
*B*1	24	(fixed values from model *B*)				(24)	1246	491
C	60	10	2	5	53	130	686	396
*C*1	24	(fixed values from model *C*)				(24)	1218	491
D	60	10	2	—	57	129	683	396
E	60	10	2	5	57	134	680	396

Model *A*, with unit occupancy factors for all atoms, refined to a discrepancy factor $r=0{\cdot}00755$ for 114 adjustable parameters. As a description of the molecular electron distribution, however, it was disappointing because it assigned negligible charges q and negative longitudinal breadth parameters c_1^2 to both exocyclic and endocyclic C–C bond clouds. This defect was remedied in models *B*, *C*, *D*, and *E* by the assignment of independent occupancy factors to all carbon and oxygen atoms, whose function was to permit a migration of charge from the atomic peaks into the bond regions. By this means physically sensible parameters were obtained for all bond clouds (Table 6) except for C=O, which showed no appreciable bond charge in agreement with the earlier difference map. The drop in r for these models was small but encouraging (Table 1).

The previous calculations, using a real free-atom f curve for hydrogen ($\lambda=1{\cdot}0$, $\mu=0$), had led to C–H bond lengths averaging under 1·0 Å. This was attributed to a polarization of the hydrogen charge density towards the carbon ligand and it was hoped that the introduction of a complex f curve, allowing explicitly for this polarization through the adjustable hybridization ratio μ, would permit the bond lengths to refine to reasonable values $\sim 1{\cdot}1$ Å. In fact, refinement of model *C* yielded a directly opposite result, with negative hybridization ratio $\mu=-0{\cdot}12$ and short C–H bond lengths $l_A=0{\cdot}96$, $l_O=0{\cdot}92$ Å (after libration corrections). Possibly the lesson to be learned is that one cannot properly allow for the effect of covalent bonding by means of a polarized hydrogen atom without a corresponding improvement in the carbon f curve. Model *B* was adopted as a simpler alternative, in which the C–H bond lengths were fixed at reasonable values, chosen so that after correction for librational shortening, due to molecular libration, methyl torsion, and zero-point C–H bending, they would approach the somewhat arbitrary values $l_A=1{\cdot}11$, $l_O=1{\cdot}07$ Å. At the same time the several vibration parameters U_a and U_n, which in model *C* had refined to values insignificant in comparison with their estimated standard deviations, were assigned fixed values (Table 5) estimated from the average C–H stretching and bending frequencies in ethane (Mizushima, 1954) and in *p*-benzoquinone (Becker, Charney & Anno, 1965).

Evaluation of the total vibration components of the hydrogen atoms and bond pseudo-atoms required a knowledge of the molecular translation and libration tensors **T** and **ω**. Rather than derive these indirectly from the carbon and oxygen atomic vibration components U^{ij}, it seemed appropriate to obtain them more directly from the X-ray intensities by making them refinable parameters in the least-squares treatment. Accordingly, the atomic components U^{ij} of carbon and oxygen were formally constrained to conform to the rigid-body hypothesis and the molecular vibration parameters T^{ij} and ω_{ij} were refined alone, all other parameters being frozen at what were nearly final values for the several models *A*, *B*, and *C*. These refinements are labelled, respectively, *A*1, *B*1, and *C*1. The intention had been to use the molecular vibration parameters from refinement *A*1 to complete the refinement of model *A*, those from *B*1 for *B*, and those from *C*1 for *C*. However, comparison of the discrepancy factors r for these six models (Table 1) showed an unexpected pattern: imposition of the rigid-body constraint on the carbon and oxygen parameters had raised r for model *A* from 0·00755 only to 0·00880, compared with increases for *B* from 0·00707 to 0·01246 and for *C* from 0·00686 to 0·01218. The inference drawn from this exceptional behavior of model *A* was twofold: the rigid-body hypothesis is a very good approximation to the truth; and the parameters U^{ij} from model *A*, with its fixed occupancy factors, rather faithfully describe this vibrational motion whereas in the other models these parameters, together with the variable occupancy factors, serve the additional function of describing changes in atomic shape due to chemical binding. The obvious next step was to continue the refinement of the molecular vibration parameters along with the 53 'other' parameters and the scale factor (model *A*2) so as to derive a final set of molecular parameters T^{ij} and ω_{ij}. These parameters were then used in the final refinements of models *B*, *C*, *D*, and *E*; in fact they differed insignificantly from the values from models *A*1, *B*1, or *C*1.

Calculations *D* and *E* represent attempts to introduce one further bit of flexibility into the model by allowing independent parameter values to the bond clouds in the chemically inequivalent bonds C(3)–C(4) and C(3)–C(5′). The results (Table 6) indicate that this extra flexibility is not particularly important and, indeed, models *C*, *D*, and *E* are all virtually identical.

No one of the several models, apparently, contains all the information to be extracted from the present study. The carbon and oxygen coordinates may be taken indifferently from any one of the models, being nearly unchanged from model to model. The vibrational motion of these atoms is best described by the rigid-body model *A*2. For a description of the electron distribution one must look to one of the more flexible models, such as *D*, whose ellipsoidal bond clouds and bogus atomic occupancy factors and vibration parameters disguise a migration of charge that remains to be unmasked. The specific problem of the hydrogen charge distribution appears to be inseparable from that of the carbon atoms; models *B*, *C*, and *D* offer alternative descriptions and there is no obvious best choice.

Molecular dimensions and vibrations

The final atomic coordinates for model *B* are listed in Table 2. Molecular dimensions, corrected for libration, are given in Table 3 and the average dimensions of the two non-equivalent molecules in Fig. 1. The r.m.s. difference between the present bond lengths, except C–H, and those reported earlier (Rabinovich &

Schmidt, 1964) is 0·005 Å. While the differences are not appreciable, some of the changes appear to reflect systematic shifts in the positions of atoms adjacent to large bond peaks.

Comparison with *p*-benzoquinone (Trotter, 1960) shows that the principal differences between the two molecules are concentrated near the methyl substituents. On replacement of hydrogen by a methyl group the two ring bonds to C(4) are each lengthened by 0·025 Å and the angle between them decreases by 2°. Both these effects could be due, in part at least, to a change in hybridization at C(4), which tends to be more symmetric when this atom is bonded to three carbon atoms rather than to two carbons and one hydrogen. If we accept the idea that a carbon atom in an asymmetric environment diverts a disproportionate share of its 2*s* orbital into C–C bonds at the expense of its C–H bonds, we may apply similar reasoning to explain also the surprising equality of the C(2)–C(4) and C(3)–C(4) bond lengths. Thus, the tetrahedral C(2) is able to use as much of its 2*s* orbital in its bond to C(4), in competition with three C–H bonds, as does the trigonal C(3), whose bond to C(4) must compete with another C–C and a C=O bond.

Table 2. *Uncorrected atomic coordinates from model B*

	x	*y*	*z*
O(1*A*)	0·1964	0·1067	−0·2214
C(2*A*)	0·0453	0·3131	−0·0294
C(3*A*)	0·1057	0·0586	−0·1191
C(4*A*)	0·0176	0·1553	−0·0092
C(5*A*)	−0·0819	0·0974	0·1014
H(6*A*)	−0·146	0·160	0·181
H(7*A*)	−0·034	0·369	0·051
H(8*A*)	0·299	0·359	−0·029
H(9*A*)	−0·108	0·329	−0·125
O(1*B*)	0·3097	0·6169	0·7194
C(2*B*)	0·4691	0·8133	0·5230
C(3*B*)	0·4006	0·5646	0·6188
C(4*B*)	0·4889	0·6549	0·5063
C(5*B*)	0·5824	0·5919	0·3961
H(6*B*)	0·647	0·650	0·315
H(7*B*)	0·539	0·865	0·439
H(8*B*)	0·634	0·864	0·615
H(9*B*)	0·219	0·829	0·527

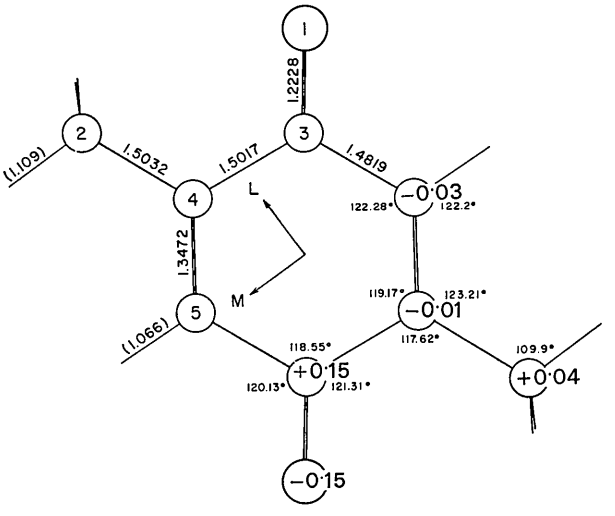

Fig. 1. Corrected molecular dimensions, from model *B*, averaged for two molecules. Figures in parentheses represent assumed values not subjected to refinement. Integer numerals in atomic circles show numbering of atoms; decimal fractions show gross atomic charges *Q*. Arrows define directions of principal inertial axes **L** and **M**.

Table 3. *Corrected molecular dimensions from model B*

Estimated standard deviations are based on coordinate covariances from inverted full least-squares matrix; they include no contribution from uncertainty in libration corrections.

Bond or angle	Molecule *A*	Molecule *B*
C=C	1·3472±0·0033 Å	1·3472±0·0033 Å
C(3)–C(4)	1·5023±0·0018	1·5011±0·0017
C(3)–C(5′)	1·4805±0·0018	1·4833±0·0018
C(2)–C(4)	1·5017±0·0018	1·5046±0·0018
C=O	1·2242±0·0022	1·2213±0·0022
O(1)–C(3)–C(4)	121·26±0·12°	121·36±0·11°
O(1)–C(3)–C(5′)	120·16±0·12	120·11±0·11
C(4)–C(3)–C(5′)	118·58±0·15	118·52±0·15
C(2)–C(4)–C(3)	117·50±0·14	117·75±0·14
C(2)–C(4)–C(5)	123·35±0·12	123·06±0·11
C(3)–C(4)–C(5)	119·15±0·11	119·19±0·11
C(4)–C(5)–C(3′)	122·27±0·12	122·29±0·11

Table 4(*a*) gives the molecular translation and libration tensors of model *A*2 as defined by their contravariant and covariant components, respectively, with respect to the dimensionless axes $\boldsymbol{\alpha}_1=|a^*|\mathbf{a}$, $\boldsymbol{\alpha}_2=|b^*|\mathbf{b}$, $\boldsymbol{\alpha}_3=|c^*|\mathbf{c}$ (Hirshfeld & Rabinovich, 1966). In Table 4(*b*) are listed the diagonal magnitudes of these tensors and the components of their unit principal axes with respect both to the dimensionless axes $\boldsymbol{\alpha}_i$ and to the respective molecular inertial axes, shown in Fig. 1. For each molecule the translation tensor is nearly diagonal in the crystal system, with its largest component along the short *a* axis, while the libration is approximately diagonal in the inertial system, being greatest about the axis of smallest moment of inertia. Apparently it is the shape of the van der Waals envelope that is important rather than the inertial tensor since in both molecules the large but not so heavy methyl groups lie nearer to the axis of maximum libration than to the smallest inertial axis.

The only internal vibration of which we have experimental evidence is the torsional oscillation of the methyl groups. This motion imparts to each hydrogen atom a tangential vibration of mean square amplitude $U_t=0{\cdot}104\pm0{\cdot}008$ Å^2, the several models all agreeing on this figure to within its e.s.d. Combining this result with the apparent C–H bond length of 0·963 Å, from model *C*, and a C–C–H angle of 109·9°, we find a torsional amplitude given by

$$\langle\sin^2\psi\rangle=0{\cdot}127\,,$$

where ψ is the torsion angle measured from the equilibrium conformation. This is a large amplitude to be treated by the harmonic approximation but we can

Table 4(*a*). *Contravariant components T^{ij} and covariant components ω_{ij} of translation and libration tensors of molecules A and B with respect to dimensionless axes $\mathbf{a}_i = |a^i|\mathbf{a}_i$*

i,j	1,1	2,2	3,3	1,2	2,3	1,3
$10^4\ T^{ij}{}_A$ (Å^2)	549	460	380	99	63	124
$10^4\ \omega_{ij,A}$ (rad^2)	54	143	64	−2	−33	−23
$10^4\ T^{ij}{}_B$ (Å^2)	543	417	365	88	33	116
$10^4\ \omega_{ij,B}$ (rad^2)	55	141	46	−28	3	−20

Table 4(*b*). *Magnitudes ($\times 10^4$) and directions of principal components of molecular translation and libration tensors* **T** *and* **ω**

Components l^i, with respect to the dimensionless axes $\mathbf{a}_i$, of unit vectors along the principal axes of **T** and **ω**, are also the direction cosines of these principal axes with respect to the reciprocal axes $\mathbf{a}^i$. Last three columns list direction cosines with respect to the respective molecular inertial axes **L**, **M**, and **N**.

	Magnitude	l^1	l^2	l^3	l_L	l_M	l_N
$T_A(1)$	550 Å^2	0·9934	0·2633	0·2670	0·2292	−0·1461	0·9623
$T_A(2)$	455	−0·1085	0·9512	0·1845	0·7076	0·7039	−0·0616
$T_A(3)$	364	−0·0386	−0·1612	0·9459	−0·6684	0·6951	0·2648
$\omega_A(1)$	148 rad^2	0·1710	0·9448	−0·2281	0·9718	0·2283	0·0587
$\omega_A(2)$	58	−0·5677	0·2659	0·6239	−0·1987	0·9272	−0·3174
$\omega_A(3)$	39	0·8053	0·1912	0·7475	−0·1270	0·2968	0·9465
$T_B(1)$	543 Å^2	−0·9998	−0·1528	−0·2257	0·1615	−0·2321	0·9592
$T_B(2)$	416	0·0150	0·9722	−0·1161	0·8055	0·5925	0·0077
$T_B(3)$	355	0·0157	−0·1775	−0·9673	−0·5701	0·7714	0·2827
$\omega_B(1)$	138 rad^2	−0·0554	0·9735	0·1137	0·9310	0·3651	0·0004
$\omega_B(2)$	52	0·7146	0·2031	−0·5232	−0·3204	0·8173	−0·4789
$\omega_B(3)$	34	−0·6973	−0·1053	−0·8446	−0·1752	0·4457	0·8779

Table 5. C–H *bond parameters from three alternative models, with estimated standard deviations based on inverted least-squares matrix*

Figures in parentheses are assumed values.

	Model *B*	Model *D*	Model *C*
Effective charge λ	1·258 ± 0·011	1·259 ± 0·013	1·279 ± 0·054
Hybridization ratio μ	0·195 ± 0·012	−0·085 ± 0·055	−0·125 ± 0·060
Aliphatic C–H:			
l_A (corrected)	(1·109 Å)	0·972 ± 0·032 Å	0·963 ± 0·034 Å
C–C–H angle	109·9 ± 0·3°	109·8 ± 0·4°	109·9 ± 0·4°
$U_{A,a}$	(0·0057 Å^2)	(0·0057 Å^2)	−0·001 ± 0·010 Å^2
$U_{A,n}$	(0·0116 Å^2)	(0·0116 Å^2)	0·021 ± 0·008 Å^2
$U_{A,t}$	0·097 ± 0·007 Å^2	0·108 ± 0·008 Å^2	0·105 ± 0·008 Å^2
Olefinic C–H:			
l_O (corrected)	(1·066 Å)	0·934 ± 0·028 Å	0·916 ± 0·030 Å
C=C–H angle	122·3 ± 0·3°	122·4 ± 0·4°	122·3 ± 0·4°
$U_{O,a}$	(0·0055 Å^2)	(0·0055 Å^2)	0·010 ± 0·010 Å^2
$U_{O,n1}$ (in-plane)	(0·0139 Å^2)	(0·0139 Å^2)	0·013 ± 0·009 Å^2
$U_{O,n2}$ (out-of-plane)	(0·0186 Å^2)	(0·0186 Å^2)	0·029 ± 0·012 Å^2

Table 6. *Charges q and Gaussian width parameters a_i^2 (Å^2) of bond pseudo-atoms from model D*

Last column lists calculated peak pseudo-atom densities $\varrho_0 = q/a_1a_2a_3(2\pi)^{3/2}$ (e.Å^{-3}).

Bond	q	$a_1{}^2$	$a_2{}^2$	$a_3{}^2$	ϱ_0
C=O	0·06 ± 0·04	0·06 ± 0·06	0·01 ± 0·03	0·54 ± 0·37	0·36
C=C	0·37 ± 0·10	0·10 ± 0·06	0·05 ± 0·01	0·20 ± 0·03	0·74
C(2)–C(4)	0·29 ± 0·10	0·32 ± 0·16	0·05 ± 0·01	0·01 ± 0·01	1·37
C(3)–C(4)	0·42 ± 0·09	0·32 ± 0·11	0·06 ± 0·01	0·04 ± 0·01	1·01
C(3)–C(5′)	0·48 ± 0·07	0·42 ± 0·07	0·03 ± 0·01	0·05 ± 0·01	1·34
⟨C–C⟩	0·40	0·35	0·04	0·03	1·11

make a rough guess of the rotational barrier if we assume a simple threefold potential and ignore what may be an appreciable sixfold component. If we take the potential to be

$$V = V_0 (1 - \cos 3\psi) ,$$

the estimated barrier is

$$2V_0 = 1{\cdot}1 \text{ kcal.mole}^{-1}$$

and the torsional frequency, in wave numbers, is

$$\nu/c = 140 \text{ cm}^{-1} .$$

The equilibrium conformation has one C–H bond in the plane of the quinone ring, eclipsing the C=C bond. This conformation is evidently weakly stabilized by repulsion between the two out-of-plane hydrogen atoms and the carbonyl oxygen. The observed methyl orientation in one of the molecules in fact departs from this symmetric conformation by $2{\cdot}9 \pm 0{\cdot}7°$ (compared to $0{\cdot}7 \pm 0{\cdot}7°$ in the other molecule); this is apparently a real deviation attributable to intermolecular forces.

Electron density

The main reason for choosing to derive the electron distribution by least-squares refinement rather than by difference Fourier synthesis is that this method allows the smearing effect of thermal vibrations to be eliminated so that the electron density in different parts of a molecule, or even in different structures, can be directly compared. The price to be paid for this benefit includes the need to postulate a definite model, incorporating a strictly limited set of adjustable parameters; if the model is poor the results obtained may be correspondingly misleading.

The model selected to represent the electron distribution has been dictated partly by chemical theory, partly by experiment, and partly by computational convenience. Theoretical studies and previous crystallographic evidence both imply that a covalently bonded hydrogen atom is more compact than a free atom and is polarized in the direction of the bond (Iijima & Bonham, 1963; Stewart, Davidson & Simpson, 1965). The particular form of density function adopted was suggested by Rosen's (1931) valence-bond wave function for the H_2 molecule. Rosen used a Heitler–London formulation based on hybrid atomic orbitals on the two atoms composed of $1s$ and $2p_z$ functions, with the $2p_z$ function contracted to have the same orbital exponent as the $1s$ function. This hybrid is of the form

$$\varphi = (\psi_s + \mu\psi_z)/(1+\mu^2)^{\frac{1}{2}} ,$$

where

$$\psi_s = (\lambda^3/\pi a_0^3)^{\frac{1}{2}} \exp(-\lambda r/a_0) ,$$

$$\psi_z = (\lambda^5/\pi a_0^5)^{\frac{1}{2}} z \exp(-\lambda r/a_0) ,$$

and the positive z axis for each atom points to the other atom. The orbital exponent λ may be regarded as the effective charge of the $1s$ orbital ψ_s (the $2p_z$ orbital ψ_z has effective charge 2λ) and μ is the hybridization ratio and measures the degree of charge polarization.

The bond pseudo-atoms also were suggested by both theoretical and experimental evidence. Theoretically, they are related to the overlap density in the covalent bond, which is proportional to the product of the atomic wavefunctions out of which the bond orbital, in either the valence-bond or the molecular-orbital approximation, is constructed. In the case of a localized σ-bond orbital this overlap density has cylindrical symmetry about the bond axis, but the presence of π-bond electrons lowers this axis to one of twofold symmetry. These expected properties, largely confirmed by the earlier difference map, were incorporated in the ellipsoidal bond clouds centred at the midpoints of the several carbon–carbon and carbon–oxygen bonds with their principal axes oriented in accordance with the local symmetry. The Gaussian profiles assumed for these bond clouds allowed them to be treated as harmonically vibrating point charges with no modification of the existing computer program. No such clouds were inserted in the C–H bonds because the difference map had shown no excess density in these regions and because it was felt that the use of polarized hydrogen atoms would provide adequate flexibility in the description of the C–H bond density.

The excess electron density in the carbon–carbon bonds implies a corresponding deficiency elsewhere. Neither theory nor experiment provides a safe guide to the spatial distribution of this electron deficiency. Molecular-orbital and valence-bond approximations acknowledge the effect by simple renormalization, which scales down the atomic orbitals uniformly by a factor sufficient to balance the overlap charge. O'Konski (1962) has briefly summarized arguments against renormalization and in favour of a selective withdrawal of charge from outer regions of the valence shell. Reasonably accurate Hartree–Fock calculations on diatomic molecules (see, *e.g.* Smith & Richardson, 1965), while confirming the presence of excess density between the bonded atoms, offer scant support for any simple renormalization scheme. Nor do they provide an obvious basis for generalizing to such situations as that of a carbon atom involved in several covalent bonds. Ruedenberg (1962) has argued that an essential feature of covalent bonding is an *increase* in electron density near the nuclei. In these circumstances the best one can do is introduce sufficient flexibility into the description of the atoms to allow at least the gross features of any likely charge distribution to be properly depicted. It is hoped that an ample degree of flexibility has been provided by the assignment to each heavy atom of an adjustable occupancy factor and six anisotropic 'vibration' parameters.

Numerical results are reported in Tables 5, 6, and 7. Table 5 lists values of the hydrogen parameters obtained from models *B*, *C*, and *D*; the two extreme models *B* and *C* are also compared graphically in Fig. 1. Model *B* is the least flexible, with the C–H bond lengths

and the vibration parameters, except U_t, fixed. In model *D* the bond lengths were refined; in model *C* these and the vibration parameters were all refined. The standard deviations of the vibration parameters indicate that model *C* is unnecessarily flexible; adjusting these parameters has made no significant difference but has increased fivefold the standard deviation of the orbital exponent λ. Model *D*, with adjustable bond lengths, does seem to have yielded results significantly different from those of model *B* though with a greatly increased standard deviation of the hybridization ratio μ. But the negative value of this ratio is difficult to interpret chemically and should probably be regarded with skepticism. This cautious attitude is reinforced by the consideration that all models have assumed harmonic linear oscillations of the atoms and such a description cannot approximate well the tangential motion of the methyl hydrogens. Since in any case, as Fig. 1 illustrates, the differences among the several models are not as pronounced as the numbers in Table 5 might suggest, we are inclined to adopt the more conservative model *B* as the most reasonable description of the C–H bond. This choice allows us to compare the parameter values $\lambda=1{\cdot}26$ and $\mu=0{\cdot}20$ with Rosen's theoretical values for H_2 at its equilibrium bond length, $\lambda=1{\cdot}17$ and $\mu=0{\cdot}10$. The comparison, especially of μ, is not strictly valid since the valence-bond approximation places an additional overlap charge on the bond axis which is not present in our model of the C–H bond. Nevertheless, the suggestion that the hydrogen atom is more concentrated and polarized in the C–H than in the H–H bond may be worthy of further examination.

The charges and width parameters of the several carbon–carbon and carbon–oxygen bond clouds, derived from model *D*, are listed in Table 6. The results from models *B*, *C*, and *E* are not appreciably different from these. As noted previously, the C=O bond cloud is inappreciable. The C–C single bonds have generally similar parameters; their average values are shown in the last line of the table. The near equality, on the average, of the lateral width parameters a_2^2 and a_3^2 shows that these bond clouds have approximate cylindrical symmetry about the bond axes. By contrast, the C=C cloud is less extended along the bond axis but much more extended, as expected, along the normal to the ring plane. Fig. 3 shows a longitudinal section through the average C–C bond cloud, calculated with lateral width parameter equal to the mean of a_2^2 and a_3^2, and two principal sections through the C=C cloud. Especially significant is the sharp concentration of the bond densities on the bond axes. It is quite impossible to simulate such highly directed maxima by hybridization of atomic 2*s* and 2*p* orbitals alone. This result is in qualitative accord with Hartree–Fock calculations on such diatomic molecules as N_2 and CO (Nesbet, 1964; Cade, Sales & Wahl, 1966), which demonstrate the need for the inclusion of a large number of valence-shell orbitals, as well as outer-shell *d* and *f* orbitals, in the basis set for an accurate L.C.A.O. expansion of the molecular orbitals. It may also account for the disappointing results obtained by Rae & Maslen (1965) with complex carbon *f* curves based on sp^2 hybrid orbitals.

If we formally resolve the C=C bond cloud into σ and π components, we find the maximum π density at a distance of 0·4 Å from its nodal plane. The total

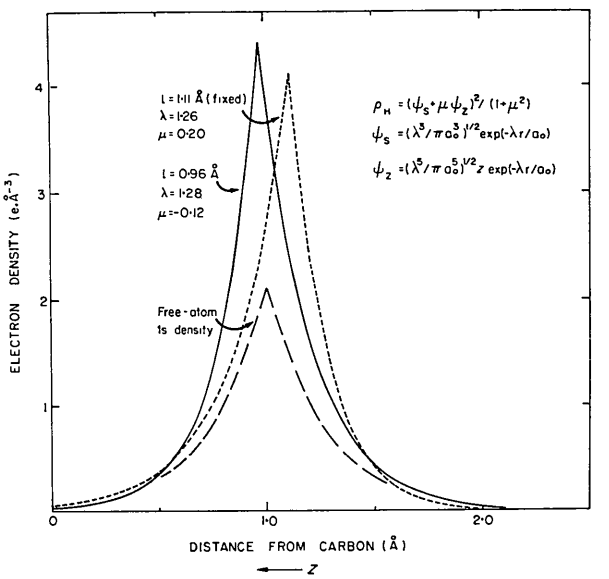

Fig. 2. Calculated hydrogen-atom electron density along C–H bond axis. Dotted line based on model *B* parameters, solid line based on model *C*. Dashed line shows free-atom density, centered arbitrarily at 1·0 Å from carbon atom.

Table 7. *Occupancy factors A, 'vibration' parameters* ΔU^{ij} (Å^2 × 10^{-4}) *referred to molecular inertial axes, and gross atomic charges Q, from model D*

	A	ΔU^{LL}	ΔU^{MM}	ΔU^{NN}	ΔU^{LM}	ΔU^{MN}	ΔU^{LN}	*Q*
O(1*A*)	1·012	1	10	10	3	−10	2	−0·13
C(2*A*)	0·966	−37	−30	−6	−4	1	−4	+0·06
C(3*A*)	0·898	−48	−42	−27	−31	7	−4	+0·13
C(4*A*)	0·904	−27	−60	−9	−15	−1	−9	+0·03
C(5*A*)	0·938	−47	−12	−6	−17	−1	14	−0·05
O(1*B*)	1·017	2	12	7	7	−6	−4	−0·17
C(2*B*)	0·973	−37	−23	−12	−5	−9	−5	+0·02
C(3*B*)	0·893	−39	−51	−47	−33	−1	−2	+0·16
C(4*B*)	0·919	−22	−54	27	−9	5	−4	−0·05
C(5*B*)	0·930	−52	−16	−2	−27	2	15	0·00

charge in the cloud splits into two quite equal shares; thus the σ component has a charge equal to $qa_2/a_3 = 0{\cdot}19$ e, scarcely half the charge in each single-bond cloud. As Fig. 3 shows, this relative poverty of the C=C σ cloud is largely accounted for by its lesser longitudinal extension, so that much of the difference between this peak and the single-bond clouds is localized near the carbon centers. Because of the strong interaction between the parameters of the bond clouds and those of the adjacent atoms, as exemplified by the behaviour of model *A*, the results cannot be interpreted as implying unambiguously a difference in strength of the two kinds of σ bond. In fact, the parameters q do not represent net excess bond charges; much of the bond-cloud charge simply replenishes the atomic densities in regions that are artificially depleted by the small occupancy factors of the carbon atoms (see below). Moreover the artificiality of the model used for the description of the bond peaks requires us to regard all quantitative conclusions as highly tentative approximations at best.

Table 7 lists, for each of the heavy atoms, the occupancy factor A and the differences ΔU^{ij}, in the appropriate molecular inertial system, between the vibration components from model *D* and those attributable to the rigid-body molecular motion of model *A*2. Immediately evident is the close similarity of the two molecules. Both oxygen atoms have occupancy factors greater than one and positive diagonal differences ΔU^{ii}, while the reverse is found for the carbon atoms. In each atom the gain or loss of charge implied by the occupancy factor is partly balanced by a broadening or sharpening of the peak, expressed in ΔU, tending to offset the change in peak density at the atomic centre. It must be remembered that the density at the atomic centres comes mainly from the inner-shell electrons and is unlikely to be greatly altered by moderate changes in the valence orbitals.

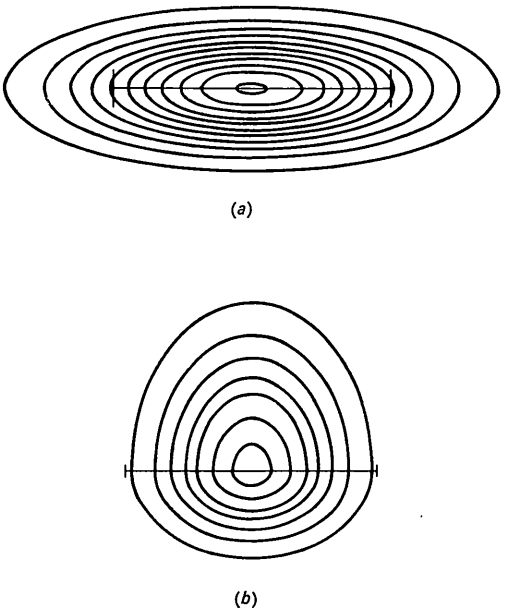

(*a*)

(*b*)

Fig. 3. Longitudinal principal sections through bond-cloud pseudo-atoms according to model *D*. Contour interval 0·1 e.Å^{-3}. Vertical strokes mark atomic positions. (*a*) C–C single bond, assuming axial symmetry ($a_2^2 = a_3^2$); (*b*) In-plane (lower half of diagram) and perpendicular (upper half) principal sections through C=C bond cloud.

The net charge on an atom of atomic number Z and occupancy factor A may be taken as $(1-A)Z$. Adding to this net charge on each atom half the charge in each of the adjacent bond clouds, we arrive at the gross atomic charges listed in Table 7, last column. Fig. 1 shows the average values for the two molecules; the estimated standard deviations of these values average 0·04 e. The only significant accumulations of charge occur at the carbonyl group and these imply a charge separation of the expected sense (C^+O^-) and reasonable magnitude.

A graphical representation of the charge distribution deduced from model *D* is shown in Fig. 4. This is a difference synthesis whose Fourier coefficients are the differences $F'_D - F_0$ between two sets of *calculated* structure factors. The set F'_D was calculated from the parameters of model *D* except that the molecular rigid-body motion and the methyl-group torsional motion have been artificially removed. Thus, the vibration parameters assigned to the heavy atoms are the differences ΔU^{ij} listed in Table 7 (except that these are referred to molecular rather than to crystal axes). Similarly the bond clouds have been given their Gaussian width parameters a_i^2 unmodified by thermal vibration and the hydrogen atoms have been given only their assumed zero-point vibrations. The set F_0 was calculated for a model comprising stationary C and O atoms, with unit occupancy factors, at the same positions as for model *D*. The hydrogen atoms were assigned the free-atom density ($\lambda = 1{\cdot}0$, $\mu = 0$), zero-point stretching and bending vibrations, and positions corresponding to the 'true' C–H bond lengths used in model *B*. Bond clouds were omitted. Ideally, then, Fig. 4 should show the charge migration in a stationary molecule compared with the undistorted atoms of which it is composed. These undistorted atoms are the ground-state hydrogen, a valence-state carbon, and a spherically averaged ground-state oxygen as implied by the *f* curves of Berghuis, Haanappel, Potters, Loopstra, MacGillavry & Veenendaal (1955).

In fact, however, this synthetic difference map suffers from some serious limitations of the model *via* which it was derived. Among the most severe: the 'vibration' parameters ΔU^{ij} that express the change of shape of the atomic peaks include many negative diagonal components, which render the Fourier series with coefficients F'_D divergent. Our procedure has been to truncate the series essentially at the limit of the Cu $K\alpha$ sphere so as to include the same terms as are represented in the experimental data. The divergent behaviour of the series actually begins to manifest itself only at a much larger reciprocal radius.

Some uncertainty, too, attaches to the molecular vibration parameters entering into the evaluation of the differences ΔU^{ij}. Our confidence in these parameters rests largely on the low value of r obtained for model $A2$, but this is no guarantee against systematic errors in the vibration tensors. For example, a uniform deformation, isotropic or anisotropic, of all five heavy atoms would simply be swallowed by the molecular translation tensor **T** and leave no trace in r or in the difference map.

One may also question the use of real f curves for the heavy atoms, which constrain the atomic contribution to the difference density to be centrosymmetric in the immediate neighborhood of each atomic center. Departures from centrosymmetry arise only through the presence of the bond-cloud pseudo-atoms, most of which (see Fig. 3) appreciably overlap the adjacent atomic centers. A simple way of additionally lowering the symmetry would have been to choose different atomic coordinates for the calculation of F'_D and F_0. But in the absence of neutron-diffraction data, which might have yielded nuclear positions (and vibration parameters) suitable for calculating F_0, we have no way of estimating any apparent atomic displacements that may have resulted from charge migration in the heavy atoms.

There is some comfort in the argument that these weaknesses of the model are more likely, on the whole, to have suppressed real features in the difference density than to have created false ones. We believe that the positions of the principal maxima and minima in Fig. 4 are significant, though their magnitudes are undoubtedly much less so.

At the centres of all heavy atoms, $\Delta\varrho$ is not far from zero. The actual values observed at these positions are highly sensitive both to the truncation of the Fourier series and to any errors in the molecular vibration tensors. An apparent effect of the former is found in difference-density sections perpendicular to the molecular planes, through the bond axes. The most prominent new features in these sections occur above and below the ring atoms at about 0·6 Å from the molecular plane and are opposite in sign to the difference densities at the atomic centers.

The positive peaks at the hydrogen positions reflect the contraction of the hydrogen atomic charge seen more clearly in Fig. 2. In agreement with that figure also, the negative difference density surrounding the hydrogen peaks is too diffuse to stand out in Fig. 4.

The C–C bonds are all marked by prominent positive features but these are much smaller, in peak density and in longitudinal extent, than the bond clouds of Fig. 3. The discrepancy must be attributed to the atomic difference-density contributions, which introduce deep hollows at the positions of all carbon atoms. These hollows, arising from the small atomic occupancy factors, reach depths of $-0{\cdot}5$ to $-1{\cdot}0$ e.Å^{-3} at the centres of the several carbon atoms. They cancel most of the positive density contributed by the bond clouds, leaving only a small residual peak, of barely 0·1 e total charge, at the middle of each C–C bond. On the opposite side of each atom, away from any bond direction, is a compact trough located 0·5 to 0·7 Å from the atomic centre. The charge removed from each of these troughs appears adequate to provide, on the average, about half the charge in each bond peak.

The sections, in the molecular planes, through the C–C and C=C bond peaks are similar in size and shape. It seems fair to regard the σ component of the double bond as essentially equivalent to a single bond,

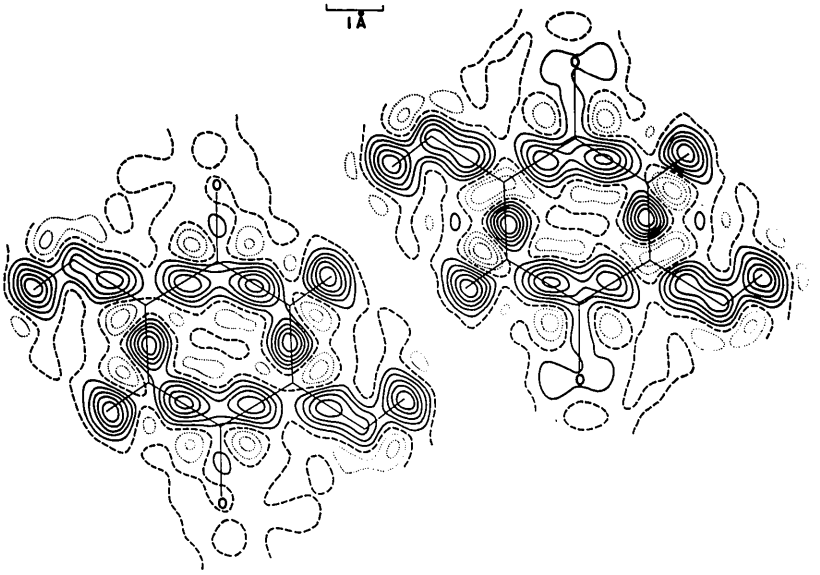

Fig. 4. Synthetic difference-density sections in mean molecular planes, based on model *D* corrected for molecular vibration. Contour interval 0·1 e.Å^{-3}, zero contour broken, negative contours dotted.

in qualitative accord with one of the basic postulates of Hückel theory.

The difference density along the normal to the molecular plane through the midpoint of each C=C bond may be regarded as a superposition of σ and π difference densities. Comparing these normal profiles with the corresponding in-plane profiles, where the π density vanishes, we can deduce the general shape of the π difference density alone. This is found to have its maximum, nearly $+0{\cdot}4$ e.Å^{-3}, about 0·5 Å from the nodal plane. The total excess charge in the π bond, like that in the σ bond, is about 0·1 e. There is no clear indication where this charge comes from.

Our general picture of the C–C σ bond shows a sharp peak of excess charge density reaching $+0{\cdot}5$ e.Å^{-3} midway between the bonded atoms. This peak contains about 0·1 e and is balanced by two small troughs on the far sides of the atoms about half a bond length from their centres. In this respect, the covalent bond may be regarded as affecting carbon and hydrogen atoms similarly, polarizing their electronic charge in the direction of the bond axis. Quantitatively, these atoms differ, apart from the contraction of charge around the hydrogen nucleus that is apparently not duplicated in carbon, in that the regions of charge depletion are much more sharply localized in carbon than in hydrogen. While this is a reasonable result, the present evidence is inconclusive since our model has not treated carbon and hydrogen equivalently.

It is reassuring to compare the present results with those obtained by other investigators using more conventional procedures. The low-temperature (100°K) study of cyanuric acid by Verschoor (1964) showed compact difference-density maxima in the C–N and C=O bonds comparable in shape to the C–C bond peaks in our Fig. 4. Similar features were also found by O'Connell, Rae & Maslen (1966) in their difference maps based on the room-temperature data of Beagley & Small (1963) for ammonium oxamate and of Cady & Larson (1965) for triaminotrinitrobenzene. These studies further agree with ours in placing discrete troughs behind the atoms on the sides opposite the covalent bonds. Especially in triaminotrinitrobenzene, where the high molecular symmetry and the small and equally symmetric vibrational motion justify the averaging of the difference density over several chemically equivalent regions in space, the average difference density in the molecular plane (O'Connell, Rae & Maslen, 1966, Fig. 4*a*) bears a close qualitative resemblance to our Fig. 4.

Dawson (1965) has considered a model of, for example, the difference density in diamond, in which each atom is surrounded by an anti-centrosymmetric array of four peaks and four troughs, the peaks overlapping in pairs on the axes of the C–C bonds. His difference density in the diamond $(1\bar{1}0)$ plane shows inner contours at $+0{\cdot}55$ and $-0{\cdot}25$ e.Å^{-3}, respectively, around the peaks and troughs, in nearly quantitative agreement with our results. The total charge in each bond peak is harder to estimate. Dawson originally gave the contribution of each atom to this peak as 0·1 to 0·15 e. In a later note (Dawson, 1966) he estimated the charge redistribution in the carbon atom at 0·087 e per bond. This is nearer to our rough estimate of 0·05 e per atom donated to each C–C bond in dimethylquinone.

Where our results differ most unexpectedly from previous studies is in the absence of any positive features near the carbonyl oxygen. In contrast to cyanuric acid, where Verschoor (1964) found sharp maxima both in the C=O bonds and in locations customarily associated with lone-pair orbitals, our difference map is surprisingly flat in the vicinity of the oxygen atoms.

The major changes in electron density in dimethylquinone attributable to chemical binding may be summarized as follows:

The C–C bond displays an excess charge of about 0·1 e in a compact peak, of maximum density 0·5 e.Å^{-3}, located between the bonded atoms. The sharp peaking of this excess density on the bond axis implies that the bonding molecular orbital requires for its L.C.A.O. expansion considerably more than a minimal set of 2*s* and 2*p* atomic orbitals.

The corresponding charge deficiency is localized in isolated troughs on the far sides of the carbon atoms; no appreciable change of density is observed at the atomic centres.

The C=C bond contains a peak of excess density elongated in the direction normal to the ring plane. This can be resolved approximately into σ and π components, the former resembling a single-bond peak. The π difference density is maximal about 0·5 Å above and below the nodal plane, where it reaches nearly $+0{\cdot}4$ e.Å^{-3}.

The C=O bond exhibits a small polarity C^+O^- but no concentrated charge accumulation or deficiency either on the bond axis or anywhere near the oxygen atom.

A hydrogen atom bonded to carbon undergoes a pronounced contraction of its charge cloud and a polarization in the direction of the bond. Both these effect appear somewhat greater than in the H_2 molecule.

All these conclusions are preliminary and require verification with better intensity data collected at lower crystal temperatures. It is hoped that improvements in experimental technique will be accompanied by advances in methods of interpretation, guided by the chemical insights gained from sophisticated theoretical studies of suitable model systems.

We gratefully acknowledge partial support of this work by contract G-53 of the National Bureau of Standards, Washington, D.C.

References

BEAGLEY, B. & SMALL, R. W. H. (1963). *Proc. Roy. Soc.* A, **275**, 469.

BECKER, E. D., CHARNEY, E. & ANNO, T. (1965). *J. Chem. Phys.* **42**, 942.

BERGHUIS, J., HAANAPPEL, IJ. M., POTTERS, M., LOOPSTRA, B. O., MACGILLAVRY, C. H. & VEENENDAAL, A. L. (1955). *Acta Cryst.* **8**, 478.
CADE, P. E., SALES, K. D. & WAHL, A. C. (1966). *J. Chem. Phys.* **44**, 1973.
CADY, H. H. & LARSON, A. C. (1965). *Acta Cryst.* **18**, 485.
CRUICKSHANK, D. W. J. (1956). *Acta Cryst.* **9**, 754.
DAWSON, B. (1965). *Austral. J. Chem.* **18**, 595.
DAWSON, B. (1966). *Acta Cryst.* **21**, A5.
HIRSHFELD, F. L. & RABINOVICH, D. (1966). *Acta Cryst.* **20**, 146.
HIRSHFELD, F. L., RABINOVICH, D., SCHMIDT, G. M. J. & UBELL, E. (1963). *Acta Cryst.* **16**, A57.
IIJIMA, T. & BONHAM, R. A. (1963). *Acta Cryst.* **16**, 1061.
MCWEENY, R. (1951). *Acta Cryst.* **4**, 513.
MIZUSHIMA, S. (1954). *Structure of Molecules and Internal Rotation*, p. 60. New York: Academic Press.
NESBET, R. K. (1964). *J. Chem. Phys.* **40**, 3619.
O'CONNELL, A. M., RAE, A. I. M. & MASLEN, E. N. (1966). *Acta Cryst.* **21**, 208.
O'KONSKI, C. T. (1962). In *Determination of Organic Structures by Physical Methods*, Vol. 2, p. 693, Nachod & Phillips, eds. New York: Academic Press.
RABINOVICH, D. & SCHMIDT, G. M. J. (1964). *J. Chem. Soc.* p. 2030.
RAE, A. I. M. & MASLEN, E. N. (1965). *Acta Cryst.* **19**, 1061.
ROSEN, N. (1931). *Phys. Rev.* **38**, 2099.
RUEDENBERG, K. (1962). *Rev. Mod. Phys.* **34**, 326.
SMITH, P. R. & RICHARDSON, J. W. (1965). *J. Phys. Chem.* **69**, 3346.
STEWART, R. F., DAVIDSON, E. R. & SIMPSON, W. T. (1965). *J. Chem. Phys.* **42**, 3175.
TROTTER, J. (1960). *Acta Cryst.* **13**, 86.
VERSCHOOR, G. C. (1964). *Nature, Lond.* **202**, 1206.

Acta Cryst. (1967). **23**, 1000

The Crystal and Molecular Structure of Magnesium Hexa-antipyrine Perchlorate

BY M. VIJAYAN AND M. A. VISWAMITRA*

Department of Physics, Indian Institute of Science, Bangalore 12, *India*

(*Received* 17 *January* 1967)

The structure of magnesium hexa-antipyrine perchlorate, $Mg(C_{11}H_{12}ON_2)_6(ClO_4)_2$, has been solved by isomorphous difference-Patterson and trial-and-error methods. The compound crystallizes in the hexagonal system, space group $P\bar{3}$, with one formula unit in a unit cell of dimensions $a=14{\cdot}06$, $c=9{\cdot}76$ Å. The positional and anisotropic thermal parameters of the atoms were refined by the method of least squares to an R value of 0·132 for 1184 observed reflexions. In the structure, the six $\bar{3}$ equivalent antipyrine molecules are coordinated octahedrally to the central Mg^{2+} ion through their lone carbonyl oxygen atoms. The pyrazolone and the phenyl rings in the antipyrine group are planar and are inclined to each other by 62·3°. The non-equivalent Cl–O distances in the structure are 1·448 and 1·437 Å.

Introduction

Antipyrine is the trivial name for 1-phenyl-2,3-dimethyl-5-pyrazolone, an important keto derivative of pyrazoline which was first synthesized by Knorr (1884). Antipyrine receives its name from the antipyretic properties which are shared by several of its derivatives. The large dipole moment of antipyrine favours its coordination to different metal ions *via* the oxygen atom in the carbonyl group. Further, the proton accepting nature of the oxygen atom facilitates the formation of hydrogen bonded complexes with proton-donor molecules and groups. A large number (over 300) of metallic and molecular compounds of antipyrine have been synthesized. However, the only structural information so far reported in the literature concerning antipyrine compounds is about $Tb(C_{11}H_{12}ON_2)_6I_3$, which crystallizes in the space group $R\bar{3}$ (Van Uitert & Soden, 1961). No further details of this investigation are available. Hence, a programme of systematic X-ray investigation of some metal antipyrine complexes was initiated to study the nature of the metal–oxygen bonding in these and also to deduce the molecular geometry of antipyrine (Vijayan & Viswamitra, 1965*a*).

The first structure to be solved in this connexion was that of magnesium hexa-antipyrine perchlorate. A preliminary note on this investigation has already been published (Vijayan & Viswamitra, 1965*b*). A complete account of the solution and the refinement of the structure is given here. The structure determination of lead hexa-antipyrine perchlorate, taken up later, has also been reported (Vijayan & Viswamitra, 1966).

Experimental

Well developed, transparent crystals of magnesium hexa-antipyrine perchlorate were grown from a solution in water or methyl cyanide by slow evaporation at room temperature, using the sample kindly supplied

* Present address: Chemical Crystallography Laboratory, South Parks Road, Oxford, England.